because we noticed that the slightest flattening of imaginal discs during mounting or observation resulted in the outgrowth of longer cellular processes. Further compression resulted in cells lying down towards the outside of the disc and stretching tremendously while maintaining basal and apical adherences before the basal lamina eventually broke. The long and straight processes observed in these conditions and referred to as cytonemes by others[30] characteristically point towards the disc centre and are not seen when the tissue is rigidified by aldehyde fixation. It is therefore our belief that these structures are 'couched-and-stretched' cells. Stained preparations were mounted in Citifluor (Agar Scientific) and imaged in the same way with a 25×/0.75, 40×/1.0 or 63×/1.4 oil-immersion lens. Sequential scanning was used for all double labelling and zooming factors, and Z steps were chosen to optimize pixel size so as to match Rayleigh resolution while avoiding aliasing. Post-acquisition median filtering and contrast adjustment of image stacks and movies were performed with Imaris software (Bitplane).

Quantitative image analysis

Photoshop (Adobe) was used to draw one-pixel-wide lines over processes, and their cumulative lengths per cell and per 60° sector were calculated by counting pixels in Image Tool (University of Texas). The number of cells potentially contacted by the filopodia web of a given SOP was counted in phalloidin-stained preparations or, because disc cells typically have five to seven neighbours, estimated by superimposing images with a hexagonal lattice five times at random per cell and in five discs. Because cell diameter varied with genotype, grid cell size was matched to the mean cell diameter, as measured in optical sections. Cells expressing the E(spl)m8-driven LacZ reporter were counted as β-Gal-positive when the fluorescence intensity in the unfiltered image was 20% or more above background. These experiments, in which discs of various genotypes were processed in parallel, were repeated five times. Significance was assessed by a Fisher exact test with the Statview software (Abacus Concepts) and results were considered significant at $P < 0.05$.

Microchaete density and macrochaete counts

Adult flies were killed at −20 °C and gold–palladium sputtered at room temperature. Thoraxes were imaged with a Hitachi S4000 scanning electron microscope at 15 kV with a working distance of 25 mm. Metamorph software (Universal Imaging) was used to count microchaetes and epidermal cells in the rectangle defined by the dorsocentral macrochaetes. Microchaete density was expressed as a percentage of the total cells and bristles. Significance was assessed by a t-test for independent samples with Statistica software (Statsoft). Macrochaetes were counted on live flies, and significance was assessed by a Fisher exact test with Genepop software (http://wbiomed.curtin.edu.au/genepop/). For both tests, results were considered significant at $P < 0.05$.

Received 10 September; accepted 28 October 2003; doi:10.1038/nature02157.

1. Huang, F., Dambly-Chaudiere, C. & Ghysen, A. The emergence of sense organs in the wing disc of *Drosophila*. *Development* **111,** 1087–1095 (1991).
2. Usui, K. & Kimura, K. Sequential emergence of the evenly spaced microchaetes on the notum of *Drosophila*. *Roux's Arch. Dev. Biol.* **203,** 151–158 (1993).
3. Lai, E. C. & Rubin, G. M. neuralized functions cell-autonomously to regulate a subset of notch-dependent processes during adult *Drosophila* development. *Dev. Biol.* **231,** 217–233 (2001).
4. Renaud, O. & Simpson, P. scabrous modifies epithelial cell adhesion and extends the range of lateral signalling during development of the spaced bristle pattern in *Drosophila*. *Dev. Biol.* **240,** 361–376 (2001).
5. Wigglesworth, V. B. Local and general factors in the development of 'pattern' in *Rhodnius prolixus* Hemiptera. *J. Exp. Biol.* **17,** 180–200 (1940).
6. Parks, A. L. & Muskavitch, M. A. Delta function is required for bristle organ determination and morphogenesis in *Drosophila*. *Dev. Biol.* **157,** 484–496 (1993).
7. Jennings, B., Preiss, A., Delidakis, C. & Bray, S. The Notch signalling pathway is required for Enhancer of split bHLH protein expression during neurogenesis in the *Drosophila* embryo. *Development* **120,** 3537–3548 (1994).
8. Lecourtois, M. & Schweisguth, F. The neurogenic suppressor of hairless DNA-binding protein mediates the transcriptional activation of the enhancer of split complex genes triggered by Notch signaling. *Genes Dev.* **9,** 2598–2608 (1995).
9. Zeng, C., Younger-Shepherd, S., Jan, L. Y. & Jan, Y. N. Delta and Serrate are redundant Notch ligands required for asymmetric cell divisions within the *Drosophila* sensory organ lineage. *Genes Dev.* **12,** 1086–1091 (1998).
10. Qi, H. *et al.* Processing of the notch ligand delta by the metalloprotease Kuzbanian. *Science* **283,** 91–94 (1999).
11. Mishra-Gorur, K., Rand, M. D., Perez-Villamil, B. & Artavanis-Tsakonas, S. Down-regulation of Delta by proteolytic processing. *J. Cell Biol.* **159,** 313–324 (2002).
12. Kooh, P. J., Fehon, R. G. & Muskavitch, M. A. Implications of dynamic patterns of Delta and Notch expression for cellular interactions during *Drosophila* development. *Development* **117,** 493–507 (1993).
13. Sanson, B., Alexandre, C., Fascetti, N. & Vincent, J. P. Engrailed and hedgehog make the range of Wingless asymmetric in *Drosophila* embryos. *Cell* **98,** 207–216 (1999).
14. Milan, M., Weihe, U., Perez, L. & Cohen, S. M. The LRR proteins capricious and Tartan mediate cell interactions during DV boundary formation in the *Drosophila* wing. *Cell* **106,** 785–794 (2001).
15. Locke, M. & Huie, P. Epidermal feet in insect morphogenesis. *Nature* **293,** 733–735 (1981).
16. Fehon, R. G. *et al.* Molecular interactions between the protein products of the neurogenic loci Notch and Delta, two EGF-homologous genes in *Drosophila*. *Cell* **61,** 523–534 (1990).
17. Bretscher, A., Edwards, K. & Fehon, R. G. ERM proteins and merlin: integrators at the cell cortex. *Nature Rev. Mol. Cell Biol.* **3,** 586–599 (2002).
18. Martin, M. *et al.* Ezrin NH_2-terminal domain inhibits the cell extension activity of the COOH-terminal domain. *J. Cell Biol.* **128,** 1081–1093 (1995).
19. Martin, M., Roy, C., Montcourrier, P., Sahuquet, A. & Mangeat, P. Three determinants in ezrin are responsible for cell extension activity. *Mol. Biol. Cell* **8,** 1543–1557 (1997).
20. Meir, E., von Dassow, G., Munro, E. & Odell, G. M. Robustness, flexibility, and the role of lateral inhibition in the neurogenic network. *Curr. Biol.* **12,** 778–786 (2002).
21. Turing, A. M. The chemical basis for morphogenesis. *Phil. Trans. R. Soc. Lond. B* **237,** 37–72 (1952).
22. Bellaiche, Y., Gho, M., Kaltschmidt, J. A., Brand, A. H. & Schweisguth, F. Frizzled regulates localization of cell-fate determinants and mitotic spindle rotation during asymmetric cell division. *Nature Cell Biol.* **3,** 50–57 (2001).
23. Lee, T. & Luo, L. Mosaic analysis with a repressible cell marker for studies of gene function in neuronal morphogenesis. *Neuron* **22,** 451–461 (1999).
24. Hinz, U., Giebel, B. & Campos-Ortega, J. A. The basic-helix–loop–helix domain of *Drosophila* lethal of scute protein is sufficient for proneural function and activates neurogenic genes. *Cell* **76,** 77–87 (1994).
25. Seugnet, L., Simpson, P. & Haenlin, M. Transcriptional regulation of Notch and Delta: requirement for neuroblast segregation in *Drosophila*. *Development* **124,** 2015–2025 (1997).
26. Haenlin, M., Kunisch, M., Kramatschek, B. & Campos-Ortega, J. A. Genomic regions regulating early embryonic expression of the *Drosophila* neurogenic gene Delta. *Mech. Dev.* **47,** 99–110 (1994).
27. Bender, L. B., Kooh, P. J. & Muskavitch, M. A. Complex function and expression of Delta during *Drosophila* oogenesis. *Genetics* **133,** 967–978 (1993).
28. Lamb, R. F. *et al.* Essential functions of ezrin in maintenance of cell shape and lamellipodial extension in normal and transformed fibroblasts. *Curr. Biol.* **7,** 682–688 (1997).
29. Andreoli, C., Martin, M., Le Borgne, R., Reggio, H. & Mangeat, P. Ezrin has properties to self-associate at the plasma membrane. *J. Cell Sci.* **107,** 2509–2521 (1994).
30. Ramirez-Weber, F. A. & Kornberg, T. B. Cytonemes: cellular processes that project to the principal signaling center in *Drosophila* imaginal discs. *Cell* **97,** 599–607 (1999).

Acknowledgements This work was initiated in the unité INSERM 432, Université Montpellier II. We thank S. Baghdiguian, C. Dambly-Chaudière, A. Ghysen, S. Layalle, P.-H. Mangeat and A.-M. Martinez for discussions; C. Dambly-Chaudière, M. Haenlin, F. Schweisguth, J.-P. Vincent, the Bloomington Stock Center and the Developmental Studies Hybridoma Bank for fly stocks and reagents; N. Lautrédou-Audouy for help with confocal microscopy; F. Mérezègue for help with electron microscopy; E. Gazave and A. Sahuquet for help with morphometry and statistics; and C. Roy for critically reading the manuscript. C.d.J. and D.A. thank the researchers into *Drosophila* at the Institut de Génétique Humaine (Montpellier) for hospitality. This work was supported by grants to D.A. from the Association pour la Recherche contre le Cancer and the Université Montpellier II. C.d.J. was supported by the Fondation pour la Recherche Médicale.

Competing interests statement The authors declare that they have no competing financial interests.

Correspondence and requests for materials should be addressed to D.A. (daniel@univ-montp2.fr).

Synaptotagmin I is necessary for compensatory synaptic vesicle endocytosis *in vivo*

Kira E. Poskanzer, Kurt W. Marek, Sean T. Sweeney & Graeme W. Davis

Department of Biochemistry and Biophysics, Program in Neuroscience, University of California, San Francisco, 513 Parnassus Avenue, San Francisco, California 94143, USA

Neurotransmission requires a balance of synaptic vesicle exocytosis and endocytosis[1]. Synaptotagmin I (Syt I) is widely regarded as the primary calcium sensor for synaptic vesicle exocytosis[2–6]. Previous biochemical data suggest that Syt I may also function during synaptic vesicle endocytosis[7–16]; however, ultrastructural analyses at synapses with impaired Syt I function have provided an indirect and conflicting view of the role of Syt I during synaptic vesicle endocytosis[3,8–10,14]. Until now it has not been possible experimentally to separate the exocytic and endocytic functions of Syt I *in vivo*. Here, we test directly the role of Syt I during endocytosis *in vivo*. We use quantitative live imaging of a pH-sensitive green fluorescent protein fused to a synaptic vesicle protein (synapto-pHluorin) to measure the kinetics of endocytosis in *sytI*-null *Drosophila*. We then combine live imaging of the synapto-pHluorins with photoinactivation of Syt I, through fluorescein-assisted light inactivation, after normal Syt I-mediated vesicle exocytosis. By inactivating Syt I only during endocytosis, we demonstrate that Syt I is necessary for the endocytosis of synaptic vesicles that have undergone exocytosis using a functional Syt I protein.

We tagged the synaptic vesicle protein n-Synaptobrevin (n-Syb) with superecliptic, pH-sensitive green fluorescent protein (GFP)[17–20]. Expression of n-Syb–synapto-pHluorin (n-Syb-pH) in *Drosophila* neurons does not alter the functional or morphological development of the neuromuscular junction (NMJ). We show that spontaneous and evoked neurotransmitter release, the electrophysiological response to a stimulus train, FM4-64 recycling, and synaptic bouton number are normal in these animals (Supplementary Fig. 1). Quantitative imaging of n-Syb-pH demonstrates a stimulus-locked, reliable increase in fluorescence intensity that decays to baseline with an average time constant ($\tau = 12.6 \pm 1.23$ s) similar to that observed at vertebrate central nervous system synapses (Fig. 1a, b; see also Supplementary Movie 1)[17,19].

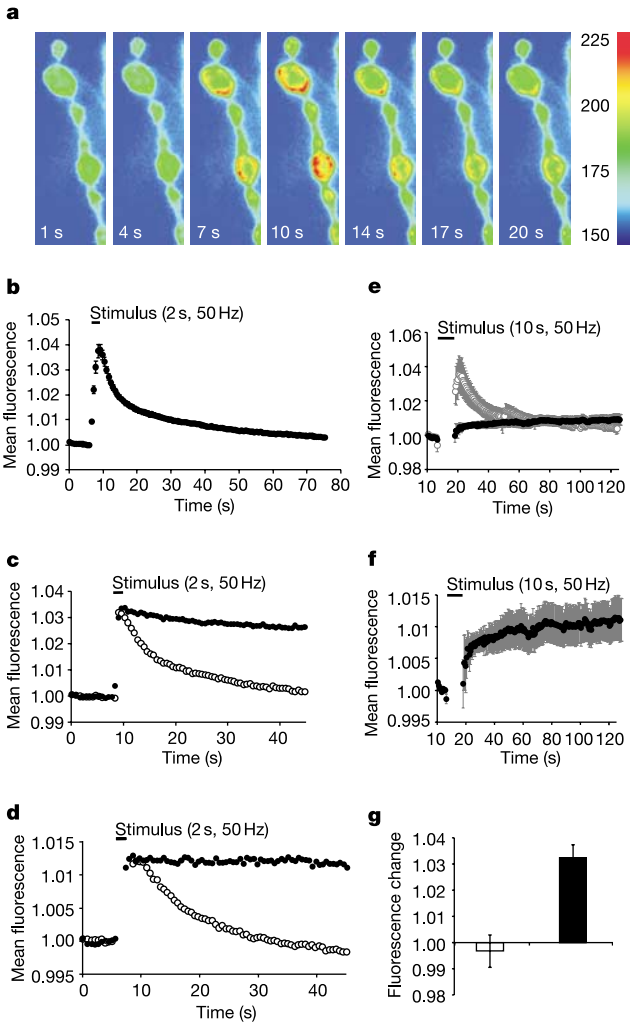

Figure 1 Endocytosis is impaired at *sytI*-null synapses. **a**, n-Syb-pH fluorescence intensity changes at the NMJ before (1 s, 4 s), during (7 s) and after (10–20 s) nerve stimulation. Scale represents arbitrary fluorescence units throughout all panels. **b**, Average n-Syb-pH fluorescence values for the synapse in **a** ($n = 7$ trials). **c**, Representative traces of n-Syb-pH intensity before (open circles) and after (filled circles) addition of bafilomycin (5 μM, 5 min incubation). **d**, n-Syb-pH intensity in a *shibire*^{ts} mutant at permissive (open circles) and restrictive (filled circles) temperatures. **e**, n-Syb-pH intensity at wild-type (open circles; $n = 4$) and *sytI*-null (filled circles; $n = 7$) synapses. **f**, n-Syb-pH intensity data at *sytI*-null synapses replotted from **e**. **g**, n-Syb-pH fluorescence change in wild-type (open bar; $n = 6$) and *sytI*-null (filled bar; $n = 5$) synapses after a 250-s, 1-Hz stimulus. Fluorescence change is calculated as the difference between pre- and post-stimulus intensities, normalized to pre-stimulus values. No images were taken during the stimulus to minimize photobleaching. *sytI*-null synapses show a significant increase in n-Syb-pH intensity ($P < 0.003$).

Additional experiments demonstrate that n-Syb-pH functions as a reliable pH-sensitive monitor of synaptic vesicle recycling at the *Drosophila* NMJ. First, n-Syb-pH shows robust changes in fluorescence intensity in response to experimental manipulation of pH (Supplementary Fig. 2a, b). Second, bafilomycin, which blocks synaptic vesicle re-acidification, inhibits the fluorescence decay after nerve stimulation, consistent with a failure to re-acidify endocytosed vesicles (Fig. 1c)[18]. Third, we generated transgenic flies harbouring n-Syb-pH and a temperature sensitive mutation in dynamin (*shibire*^{ts}). At the permissive temperature, n-Syb-pH fluorescence exhibits a wild-type, stimulus-dependent increase and decay. However, at the restrictive temperature the stimulus-dependent increase in n-Syb-pH fluorescence does not decay, consistent with the complete block of synaptic vesicle endocytosis that has been documented in *shibire*^{ts} (Fig. 1d)[21]. This endocytic block is reversible after shifting to the permissive temperature (data not shown).

To test the function of Syt I during endocytosis, we first used n-Syb-pH to measure the kinetics of endocytosis at the NMJ of *sytI*-null flies. In these experiments the stimulus-dependent (50 Hz for 10 s) increase in n-Syb-pH fluorescence is significantly less in the *sytI*-null synapses compared with controls, consistent with previous electrophysiological data (Fig. 1e, f)[2,3,22,23]. Furthermore, n-Syb-pH fluorescence after stimulation at the *sytI*-null NMJ does not decay, suggesting a severe impairment of vesicle endocytosis (Fig. 1e, f). If endocytosis is impaired in the *sytI*-null flies then we also expect persistent, low-frequency stimulation to cause a gradual accumulation of n-Syb-pH at the synaptic plasma membrane. Therefore, we stimulated wild-type and *sytI*-null synapses (1 Hz for 250 s) and imaged n-Syb-pH fluorescence before and after the stimulus train. We observed a statistically significant increase in n-Syb-pH fluorescence only at the *sytI*-null synapses, indicating that n-Syb-pH has not been efficiently recycled in the *sytI*-null flies (Fig. 1g). Although these data are consistent with a role for Syt I during vesicle endocytosis, stimulus-evoked exocytosis is severely impaired in the *sytI*-null animals, and we do not know the nature of the Syt I-independent vesicular release that remains.

To test the function of Syt I during endocytosis without affecting Syt I-mediated exocytosis, we pursued experiments to photoinactivate Syt I rapidly after normal stimulus-dependent exocytosis. We have shown previously that fluorescein-assisted light inactivation (FlAsH-FALI) is an efficient and specific method for the photoinactivation of Syt I[24]. Briefly, Syt I is tagged with a 17-amino-acid tetracysteine motif (Syt I4C) that covalently binds the membrane-permeable fluorescein derivative 4′,5′-bis(1,3,2-dithioarsolan-2-yl)fluorescein (FlAsH)[25,26]. Neuronal expression of Syt I4C rescues the *sytI*-null mutation, even when bound to the FlAsH ligand[24]. Epifluorescent illumination of FlAsH-bound Syt I4C decreases the evoked release in seconds, demonstrating efficient fluorophore-assisted light inactivation (FALI). FlAsH-FALI of Syt I4C does not alter sucrose-evoked release, demonstrating the specificity of Syt I4C photoinactivation[24]. We have now combined FlAsH-FALI of Syt I4C with the n-Syb-pH technique. To ensure that endogenous Syt I does not affect our results, Syt I4C is always expressed in a *sytI*-null mutant background. As both FlAsH and n-Syb-pH fluoresce in the green spectrum, we took advantage of the fact that epitope-bound FlAsH bleaches three orders of magnitude more rapidly than n-Syb-pH (Supplementary Fig. 2c). Epifluorescent illumination of FlAsH for 2 min decreases the FlAsH signal to near extinction, allowing us to quantitatively image n-Syb-pH.

In the first FlAsH-FALI experiment we used *shibire*^{ts} to block synaptic vesicle endocytosis conditionally and trap vesicles at the plasma membrane that have fused in the presence of functional Syt I4C during stimulation at the restrictive temperature. We then photoinactivated Syt I4C for 2 min, before shifting the preparation to the permissive temperature. If Syt I is necessary for endocytosis, we expect that n-Syb-pH will be retained at the plasma membrane

after the shift to the permissive temperature and the release of the *shibire*^{ts} endocytic block (Fig. 2a). In these experiments n-Syb-pH fluorescence is quantified at the beginning of the shift to the permissive temperature ($t = 0$). A previous ultrastructural study monitored endocytosis at multiple time points in *shibire*^{ts} flies after a shift to the permissive temperature[21]. These previous data showed that endocytosis, after release from a dynamin block, occurs at the order of several minutes, which is slower than that observed after a short stimulus in wild-type flies (see Fig. 1). The slow rate of endocytosis after release from a dynamin block may be caused by the abundance of membrane and vesicle proteins that are trapped at the plasma membrane during the endocytic block.

In this experiment we used transgenic *Drosophila* flies that harbour the *shibire*^{ts} mutation as well as neuronally driven Syt I4C and neuronally driven n-Syb-pH in a *sytI*-null background. These animals were raised at the permissive temperature, and show normal vesicle recycling at this temperature (Supplementary Fig. 2d). In our control condition stimulation at the restrictive temperature in the absence of FlAsH induces a stable increase in n-Syb-pH fluorescence that decays upon shift to the permissive temperature, reflecting normal endocytosis (Fig. 2b, c; see also Supplementary Fig. 3, control). This control experiment includes a 2-min illumination before the shift to the permissive temperature to control for the effects of illumination. Our experimental condition includes the presence of FlAsH ligand and a 2-min illumination before the shift to the permissive temperature to induce photoinactivation of Syt I4C. In this experiment the n-Syb-pH signal does not decay on shifting to the permissive temperature, indicating that Syt I4C photoinactivation significantly impairs endocytosis (Fig. 2b, c; see also Supplementary Fig. 3, FlAsH). To determine whether FlAsH fluorescence confounds our assay of endocytosis, we quantified the total synaptic n-Syb-pH fluorescence by the addition of membrane-permeable, high pH NH_4Cl saline (pH 7.4) at the end of each experiment (see Supplementary Fig. 2b). The total n-Syb-pH fluorescence is identical in control and experimental conditions, indicating that FlAsH bleaches to near extinction in these experiments (Fig. 2c). Thus, the lack of n-Syb-pH fluorescence change after Syt I4C photoinactivation cannot be attributed to additional fluorescence contributed by the presence of the FlAsH ligand. These results demonstrate that photoinactivation of Syt I4C blocks the endocytosis of synaptic vesicles that have fused with the plasma membrane using a previously functional Syt I4C molecule.

In a second FlAsH-FALI experiment we tested whether Syt I4C photoinactivation blocks endocytosis without previously pausing the vesicle cycle using *shibire*^{ts}. Here, we assayed the retention of n-Syb-pH at the synaptic plasma membrane after Syt I4C photoinactivation. FlAsH-FALI of Syt I4C was initiated at the time of stimulation (50 Hz for 5 s) and lasted for 3 min (Fig. 3a). If Syt I4C photoinactivation blocks endocytosis that normally occurs during and after the stimulus, then we expect to observe increased fluorescence at the end of the 3-min period due to unrecycled n-Syb-pH retained at the synaptic plasma membrane. We also expect to see a greater decrease in n-Syb-pH fluorescence after an acid wash, which should quench the surface n-Syb-pH fluorescence (Supplementary Fig. 2a)[18]. In this protocol, Syt I4C-dependent exocytosis will decline during the stimulation owing to photoinactivation of Syt I4C, so that the total amount of exocytosis will be less in the experimental flies compared with controls[24]. However, this will cause us to underestimate any potential difference in the accumulation of surface n-Syb-pH caused by Syt I4C photoinactivation

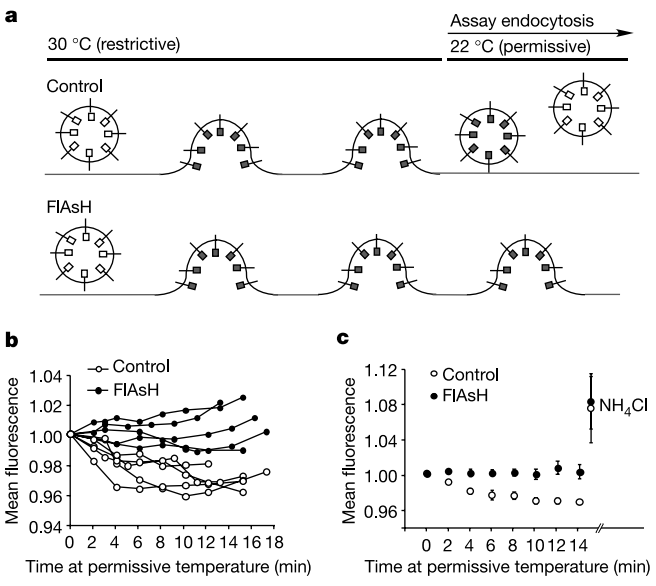

Figure 2 Photoinactivation of Syt I4C impairs endocytosis after normal vesicle fusion. **a**, Schematic of the experimental protocol and results. **b**, Quantification of the n-Syb-pH intensity changes after shift from restrictive to permissive temperatures. Each line represents a single trial from a different animal. Values are normalized to the first time point after shift to the permissive temperature. **c**, Mean values for data in **b**. Data are binned in 2-min intervals. The last point (NH_4Cl) is the intensity after addition of NH_4Cl saline at the conclusion of each trial.

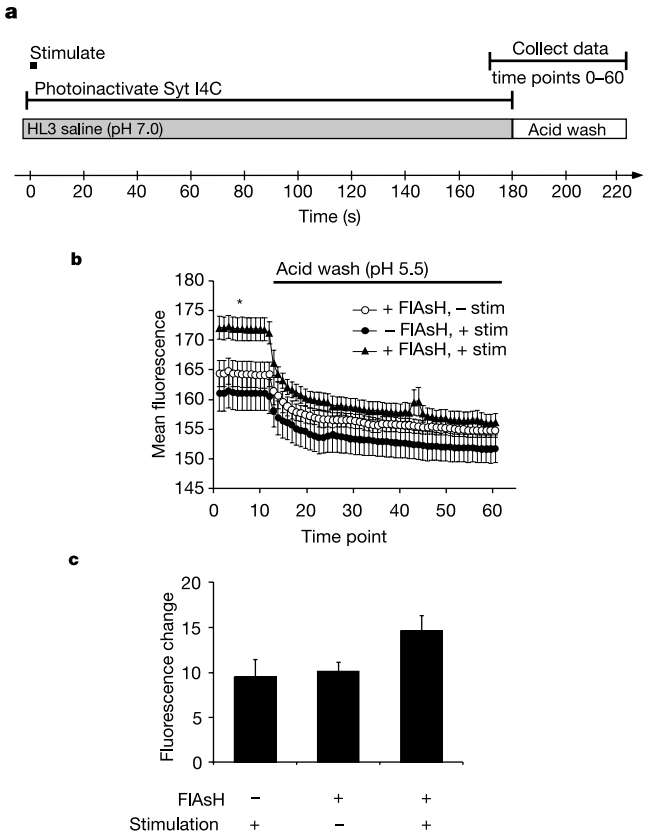

Figure 3 n-Syb-pH remains on the synaptic plasma membrane after FlAsH-FALI of Syt I4C. **a**, Protocol for acid wash experiments. **b**, Data shown include the ten time points before addition of the acid wash and the subsequent 50 time points. **c**, Change in intensity from the mean of the first ten points to the mean of the last ten in **b**. Conditions include the presence (+) or absence (−) of FlAsH ligand and presence or absence of stimulation (5 s, 50 Hz). Synapses with Syt I4C photoinactivation and stimulation ($n = 11$) show a significantly greater change in fluorescence intensity than FlAsH alone ($n = 9$, $P < 0.01$) or stimulation alone ($n = 12$, $P < 0.01$, *t*-test). Controls are not significantly different from each other. The genotype used is *syt*^{AD4}, *UAS-syt4C/syt*^{D27}; *UAS-n-Syb-pH/elaV*^{3E1}.

compared with controls. As a control, we demonstrated that n-Syb-pH recycles normally in this genetic background (Supplementary Fig. 2d).

In these experiments Syt I4C photoinactivation results in a statistically significant increase in surface n-Syb-pH fluorescence, consistent with impaired endocytosis. We quantified n-Syb-pH fluorescence 10 s before application of the acid wash (Fig. 3a). At this time n-Syb-pH intensity is significantly greater at synapses that have received both stimulation and Syt I4C photoinactivation compared with controls (Fig. 3b, asterisk). Subsequent acid wash reduced n-Syb-pH fluorescence to statistically similar levels in all conditions (Fig. 3b). Therefore, the decrease in surface fluorescence after acid wash is significantly greater at experimental synapses compared with controls (Fig. 3c). These data are consistent with a requirement of Syt I during compensatory endocytosis. Furthermore, these data argue against the possibility that Syt I functions exclusively during vesicle re-acidification, as we have assayed the plasma membrane retention of n-Syb-pH.

Finally, we measured FM4-64 uptake as an alternative assay of vesicle endocytosis. We first demonstrated normal FM4-64 loading and unloading at the *Drosophila* NMJ (Fig. 4b)[27]. We then took advantage of the fact that endocytosis is slow compared with exocytosis, allowing temporal separation of these processes. First, we stimulated (30 Hz for 1 min) synapses in the presence of FM4-64, causing similar exo- and endocytosis in all conditions. After the stimulus, vesicles will cease exocytosis, but will continue to endocytose, compensating for the large amount of release that occurred during the stimulation. We continued to bathe the synapses in FM4-64 while illuminating for 2 min. This allowed the nerve terminal to endocytose the dye during Syt I4C photoinactivation. After washing the FM4-64 away, we measured the amount of FM4-64 taken up during this endocytic phase of the experiment (Fig. 4a). If Syt I is necessary for compensatory endocytosis then we expect to observe less loading of the nerve terminal in Syt I4C-photoinactivated synapses. FlAsH-FALI of Syt I4C results in statistically lower mean fluorescence values of FM4-64 compared with controls, indicating that Syt I4C photoinactivation impairs endocytosis (Fig. 4c). We observed control levels of FM4-64 loading in the presence of FlAsH-bound Syt I4C without any illumination, demonstrating that the ligand-bound Syt I4C itself does not impair endocytosis.

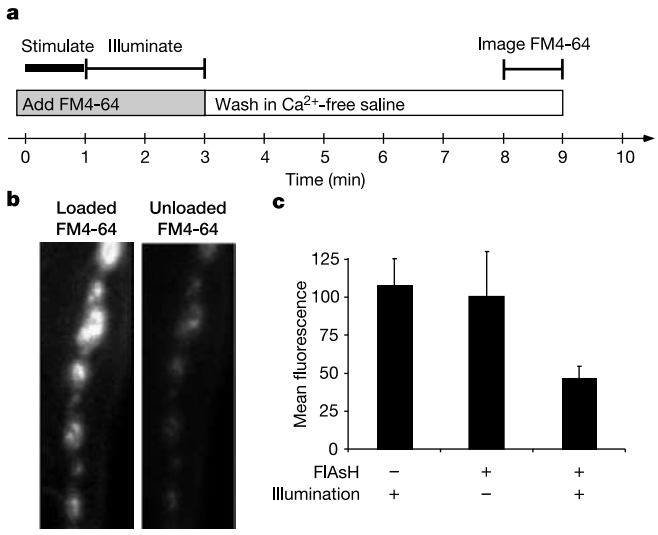

Figure 4 Photoinactivation of Syt I4C impairs stimulus-dependent FM4-64 loading at the NMJ. **a**, Protocol for FM4-64 experiments. **b**, Images demonstrating efficient loading (left) and unloading (right) of FM4-64. **c**, Quantification of FM4-64 loading at synapses in the presence (+) or absence (−) of FlAsH ligand and in the presence or absence of illumination. Loading of FM4-64 is significantly less ($P < 0.02$) at synapses that have undergone photoinactivation of Syt I4C (plus FlAsH, plus illumination, $n = 6$) compared with controls (minus FlAsH, plus illumination, $n = 7$; plus FlAsH, minus illumination, $n = 8$).

Thus, by temporally uncoupling exo- and endocytosis, we have found an essential role for a known exocytic protein (Syt I) during endocytosis. Although different modes of endocytosis with different time courses may exist[19,28,29], a specialized form of clathrin-mediated endocytosis, termed compensatory endocytosis, participates in the maintenance of the synaptic vesicle pool[1,19]. Compensatory endocytosis involves the formation of synaptic vesicles that are surrounded by clathrin and the AP-2 adaptor complex, as well as associated adaptor proteins[1]. Our data are consistent with a model based on previous biochemical data suggesting that Syt I nucleates the formation of clathrin-coated vesicles by serving as a synaptic plasma membrane docking site for the AP-2 complex[7,11–13,15,16]. This model provides a means to link the extent of synaptic vesicle exocytosis and endocytosis. Finally, it has been demonstrated that multiple Syt proteins can bind AP-2 (ref. 30). However, as we have disrupted acutely Syt I, there should not be an opportunity for other Syt proteins to bind AP-2 and nucleate endocytosis in our experiments. □

Methods

Construction of UAS-n-Syb-pH

Superecliptic pHluorin GFP was obtained from D. DeAngelis and J. Rothman. To fuse the pHluorin GFP to the carboxy terminus of n-Syb, a BsrB1 site was added to the 3′ end of an n-Syb complementary DNA (from T. Schwarz) using the oligonucleotides 5′ n-Syb (ACAGCCGAATTCGCTGAGGC) and 3′ n-Syb-BsrB1 (CCAATTAGATCTCCGCTCA CGCCGCCGTGATCGCC). An *Xba*1 site was added to the 3′ end and a BsrB1 site was added to the 5′ end of the pHluorin GFP using the oligonucleotides 5′ GFP-BsrB1 (CACGGCGGCGTGGAGCGGCGGAAGCGGCGGG) and 3′ GFP-Xba (TAGCTTCTAG ATTAACCGGTTTTGTATAG). Polymerase chain reaction fragments were then digested with BsrB1 and ligated together. The appropriate fragment was purified and used as a template for a second round of polymerase chain reaction using the oligonucleotides 5′ n-Syb and 3′ GFP-Xba. The resulting product was then digested with *Eco*R1 and *Xba*1 and ligated into pUAST. The resulting clone was sequenced before injecting into *yw* embryos.

Flies

The *UAS-n-Syb-pH* transgene was recombined with $elaV^{3E1}$-*GAL4*, and balanced with a TM6b chromosome. For the $shibire^{ts}$ experiments, w^{-}, shi^{ts2} was crossed to *UAS-n-Syb-spH*,$elaV^{3E1}$/*TM6b* and male larvae were selected against TM6b. The *sytI*-null flies were made by crossing syt^{AD4}/*CyO-GFP*; *UAS-n-Syb-pH/TM6b* to syt^{D27}/*Cyo-GFP*;$elaV^{3E1}$/*TM6b* and selecting against TM6b and Cyo-GFP expression. For the FlAsH-FALI experiments, syt^{AD4}, *UAS-syt4C/CyO-GFP*; *UAS-n-Syb-pH/TM6b* was crossed to syt^{D27}/*CyO-GFP*;$elaV^{3E1}$/*TM6b* and larvae were selected against CyO-GFP expression. The FlAsH-FALI $shibire^{ts}$ experiments were performed by crossing w^{-},shi^{ts2};syt^{D27}/*CyO-GFP*;$elaV^{3E1}$/*TM6b* to syt^{AD4}, *UAS-syt4C/CyO-GFP*;*UAS-n-Syb-pH/TM6b* and selecting males against CyO-GFP and TM6b expression.

Solutions

Third instar *Drosophila* larvae were dissected in Ca^{2+}-free HL3 saline, supplemented with calcium and adjusted to pH 7.0 (ref. 24). All experiments were performed in 0.5 mM Ca^{2+} with the exception of experiments in Fig. 1e–g, which were performed in 2.0 mM Ca^{2+}. For FlAsH experiments, dissected animals were either incubated in FlAsH solution (Invitrogen) or in a mock-FlAsH solution, then rinsed to remove unbound FlAsH[24]. Larvae were transferred back to HL3 saline before imaging. HL3 saline was adjusted to pH 5.5 in the acid wash experiments. Ammonium chloride (NH_4Cl) HL3 saline was made by replacing 50 mM NaCl with NH_4Cl and adjusting to pH 7.4.

Imaging and analysis

Images were captured on a Zeiss Axioskop 2 microscope with a water-immersion objective (× 100, 0.97 N.A.) using SlideBook software (Intelligent Imaging Innovations). Images were acquired with a Quantix cooled CCD camera including a back-thinned EEV57 chip (Roper Scientific). Illumination was provided by a 175 W xenon arc lamp and GFP or CY3 filter sets. Time-lapse imaging (500 ms exposures) was used to measure the fast time course of fluorescence changes (Figs 1, 3). Data were quantified by defining a region of interest including multiple synaptic boutons (each bouton contains multiple active zones) using the threshold function of SlideBook. The mean fluorescence intensity of this region was calculated for each time point. FlAsH-FALI was performed by illuminating the preparations as for fluorescence imaging. The NMJ at muscles 6 and 7 in segments A2–A4 were selected in all experiments. In all experiments scale represents arbitrary fluorescence units. Data are expressed as average ± standard error of the mean.

Acid wash experiments

Synapses were stimulated at the segmental nerve for 5 s at 50 Hz in 2.0 mM Ca^{2+} and imaged for 3 min before the HL3 saline (pH 7.0) in the bath was replaced with low pH acid wash (pH 5.5).

FM4-64 experiments

A total of 10 μM FM4–64 (Molecular Probes) was made in HL3 plus 0.5 mM Ca^{2+} saline and added to the bath. The nerve was stimulated for 1 min at 30 Hz. The synapse was then illuminated for 2 min. The preparation was washed repeatedly in Ca^{2+}-free HL3 for 5 min, and an image of the synapse was captured. To analyse FM4-64 uptake the n-Syb-pH fluorescence in the green channel was used to define the region of interest, and the mean intensity of the fluorescence in the red channel defined by this region was calculated. We selected a small region of interest over the muscle background and the mean intensity of this region was subtracted from the synapse intensity to correct for variability in background FM4-64 levels.

shibire^{ts} experiments

Temperature was controlled by a heating/cooling stage with a Peltier module (Brook Industries) and monitored with a temperature probe in the imaging chamber. In Fig. 1d the nerve was stimulated identically (2 s, 50 Hz) at the permissive (22 °C) and restrictive temperatures (30 °C). In the FlAsH experiments (Fig. 2) we stimulated at the restrictive temperature (2 s, 50 Hz, in HL3) every 10 s for 200 s to deplete synaptic vesicles. After stimulation, the synapse was illuminated for 2 min. The chamber was then brought down to the permissive temperature. Images of the synapse were taken at about 2 min intervals after return to the permissive temperature, and the mean intensity of the synapse was measured at each time point.

Received 25 July; accepted 6 November 2003; doi:10.1038/nature02184.
Published online 23 November 2003.

1. Jarousse, N. & Kelly, R. B. Endocytotic mechanisms in synapses. *Curr. Opin. Cell Biol.* **13,** 461–469 (2001).
2. Fernandez-Chacon, R. *et al.* Synaptotagmin I functions as a calcium regulator of release probability. *Nature* **410,** 41–49 (2001).
3. Geppert, M. *et al.* Synaptotagmin I: a major Ca^{2+} sensor for transmitter release at a central synapse. *Cell* **79,** 717–727 (1994).
4. Littleton, J. T., Stern, M., Schulze, K., Perin, M. & Bellen, H. J. Mutational analysis of *Drosophila* synaptotagmin demonstrates its essential role in Ca(2 +)-activated neurotransmitter release. *Cell* **74,** 1125–1134 (1993).
5. Perin, M. S., Fried, V. A., Mignery, G. A., Jahn, R. & Sudhof, T. C. Phospholipid binding by a synaptic vesicle protein homologous to the regulatory region of protein kinase C. *Nature* **345,** 260–263 (1990).
6. Brose, N., Petrenko, A. G., Sudhof, T. C. & Jahn, R. Synaptotagmin: a calcium sensor on the synaptic vesicle surface. *Science* **256,** 1021–1025 (1992).
7. Fergestad, T. & Broadie, K. Interaction of stoned and synaptotagmin in synaptic vesicle endocytosis. *J. Neurosci.* **21,** 1218–1227 (2001).
8. Jorgensen, E. M. *et al.* Defective recycling of synaptic vesicles in synaptotagmin mutants of *Caenorhabditis elegans*. *Nature* **378,** 196–199 (1995).
9. Littleton, J. T. *et al.* Synaptotagmin mutants reveal essential functions for the C2B domain in Ca^{2+}-triggered fusion and recycling of synaptic vesicles *in vivo*. *J. Neurosci.* **21,** 1421–1433 (2001).
10. Reist, N. E. *et al.* Morphologically docked synaptic vesicles are reduced in synaptotagmin mutants of *Drosophila*. *J. Neurosci.* **18,** 7662–7673 (1998).
11. Jarousse, N. & Kelly, R. B. The AP2 binding site of synaptotagmin 1 is not an internalization signal but a regulator of endocytosis. *J. Cell Biol.* **154,** 857–866 (2001).
12. Zhang, J. Z., Davletov, B. A., Sudhof, T. C. & Anderson, R. G. Synaptotagmin I is a high affinity receptor for clathrin AP-2: implications for membrane recycling. *Cell* **78,** 751–760 (1994).
13. Haucke, V. & De Camilli, P. AP-2 recruitment to synaptotagmin stimulated by tyrosine-based endocytic motifs. *Science* **285,** 1268–1271 (1999).
14. Fukuda, M. *et al.* Role of the C2B domain of synaptotagmin in vesicular release and recycling as determined by specific antibody injection into the squid giant synapse preterminal. *Proc. Natl Acad. Sci. USA* **92,** 10708–10712 (1995).
15. Haucke, V., Wenk, M. R., Chapman, E. R., Farsad, K. & De Camilli, P. Dual interaction of synaptotagmin with mu2- and alpha-adaptin facilitates clathrin-coated pit nucleation. *EMBO J.* **19,** 6011–6019 (2000).
16. von Poser, C. *et al.* Synaptotagmin regulation of coated pit assembly. *J. Biol. Chem.* **275,** 30916–30924 (2000).
17. Sankaranarayanan, S. & Ryan, T. A. Real-time measurements of vesicle-SNARE recycling in synapses of the central nervous system. *Nature Cell Biol.* **2,** 197–204 (2000).
18. Sankaranarayanan, S. & Ryan, T. A. Calcium accelerates endocytosis of vSNAREs at hippocampal synapses. *Nature Neurosci.* **4,** 129–136 (2001).
19. Gandhi, S. P. & Stevens, C. F. Three modes of synaptic vesicular recycling revealed by single-vesicle imaging. *Nature* **423,** 607–613 (2003).
20. Miesenbock, G., De Angelis, D. A. & Rothman, J. E. Visualizing secretion and synaptic transmission with pH-sensitive green fluorescent proteins. *Nature* **394,** 192–195 (1998).
21. Koenig, J. H. & Ikeda, K. Synaptic vesicles have two distinct recycling pathways. *J. Cell Biol.* **135,** 797–808 (1996).
22. Loewen, C. A., Mackler, J. M. & Reist, N. E. *Drosophila* synaptotagmin I null mutants survive to early adulthood. *Genesis* **31,** 30–36 (2001).
23. Yoshihara, M. & Littleton, J. T. Synaptotagmin I functions as a calcium sensor to synchronize neurotransmitter release. *Neuron* **36,** 897–908 (2002).
24. Marek, K. W. & Davis, G. W. Transgenically encoded protein photoinactivation (FlAsH-FALI): acute inactivation of synaptotagmin I. *Neuron* **36,** 805–813 (2002).
25. Griffin, B. A., Adams, S. R. & Tsien, R. Y. Specific covalent labeling of recombinant protein molecules inside live cells. *Science* **281,** 269–272 (1998).
26. Gaietta, G. *et al.* Multicolor and electron microscopic imaging of connexin trafficking. *Science* **296,** 503–507 (2002).
27. Kuromi, H. & Kidokoro, Y. Two distinct pools of synaptic vesicles in single presynaptic boutons in a temperature-sensitive *Drosophila* mutant, shibire. *Neuron* **20,** 917–925 (1998).
28. Aravanis, A. M., Pyle, J. L. & Tsien, R. W. Single synaptic vesicles fusing transiently and successively without loss of identity. *Nature* **423,** 643–647 (2003).
29. Verstreken, P. *et al.* Endophilin mutations block clathrin-mediated endocytosis but not neurotransmitter release. *Cell* **109,** 101–112 (2002).
30. Li, C. *et al.* Ca(2 +)-dependent and -independent activities of neural and non-neural synaptotagmins. *Nature* **375,** 594–599 (1995).

Supplementary Information accompanies the paper on **www.nature.com/nature**.

Acknowledgements We thank M. Ramaswami and I. Robinson for *Drosophila* stocks, and D. DeAngelis, J. Rothman and R. Kelly for the superecliptic pHluorin GFP construct. We also thank E. Heckscher for comments on an earlier version of the manuscript.

Competing interests statement The authors declare that they have no competing financial interests.

Correspondence and requests for materials should be addressed to G.W.D. (gdavis@biochem.ucsf.edu).

Lipid packing sensed by ArfGAP1 couples COPI coat disassembly to membrane bilayer curvature

Joëlle Bigay[1], Pierre Gounon[2], Sylviane Robineau[1] & Bruno Antonny[1]

[1]*Institut de Pharmacologie Moléculaire et Cellulaire, CNRS, 660 route des Lucioles, 06560 Valbonne-Sophia-Antipolis, France*
[2]*Centre Commun de Microscopie Appliquée, Université de Nice, Parc Valrose, 06103 Nice cedex 2, France*

Protein coats deform flat lipid membranes into buds and capture membrane proteins to form transport vesicles[1–3]. The assembly/disassembly cycle of the COPI coat on Golgi membranes is coupled to the GTP/GDP cycle of the small G protein Arf1. At the heart of this coupling is the specific interaction of membrane-bound Arf1–GTP with coatomer, a complex of seven proteins that forms the building unit of the COPI coat[4–7]. Although COPI coat disassembly requires the catalysis of GTP hydrolysis in Arf1 by a specific GTPase-activating protein (ArfGAP1)[8–10], the precise timing of this reaction during COPI vesicle formation is not known. Using time-resolved assays for COPI dynamics on liposomes of controlled size, we show that the rate of ArfGAP1-catalysed GTP hydrolysis in Arf1 and the rate of COPI disassembly increase over two orders of magnitude as the curvature of the lipid bilayer increases and approaches that of a typical transport vesicle. This leads to a model for COPI dynamics in which GTP hydrolysis in Arf1 is organized temporally and spatially according to the changes in lipid packing induced by the coat.

We reported previously that a fragment of ArfGAP1 (amino acids 1–257), which includes the catalytic zinc-finger domain, and Gcs1p, a yeast ArfGAP1 homologue, bind preferentially to liposomes containing conical lipids versus cylindrical lipids[11]. The binding increased gradually as the size of lipid polar heads decreased and as the cross-section of the acyl chains increased. Because the marked preference of [1–257]ArfGAP1 for conical lipids correlated with its activity on liposome-bound Arf1–GTP[11], we suggested that a loose lipid packing favours the positioning of ArfGAP1 towards membrane-bound Arf1–GTP. Similar effects of the balance between conical and cylindrical lipids were observed